

# Thermoelectric effect in the Kondo dot side-coupled to a Majorana fermion

Heunghwan Khim

*Department of Physics, Korea University, Seoul 136-701, Korea*

Rosa López

*Institut de Física Interdisciplinar i de Sistemes Complexos IFISC (CSIC-UIB), E-07122 Palma de Mallorca, Spain and  
Departament de Física, Universitat de les Illes Balears, E-07122 Palma de Mallorca, Spain*

Jong Soo Lim

*School of Physics, Korea Institute for Advanced Study, Seoul 130-722, Korea*

Minchul Lee\*

*Department of Applied Physics, College of Applied Science, Kyung Hee University, Yongin 446-701, Korea  
(Dated: November 8, 2021)*

We investigate the linear thermoelectric response of an interacting quantum dot side-coupled by one of two Majorana fermions (MFs) formed at the ends of a topological superconducting wire. We employ the numerical renormalization group technique to obtain the thermoelectrical conductance  $L$  as well as the electrical conductance  $G$  when the background temperature  $T$  and the dot gate are tuned. We distinguish two transport regimes in which  $L$  displays different features: the weak- ( $\Gamma_m < T_K$ ) and strong-coupling ( $\Gamma_m > T_K$ ) regimes, where  $\Gamma_m$  and  $T_K$  are the Majorana-dot coupling and the Kondo temperature, respectively. For an ideal (infinitely long) nanowire where the Majorana end states do not overlap ( $\epsilon_m = 0$ ), the thermoelectrical conductance  $L$  in the weak-coupling regime exhibits a peak at  $T \sim \Gamma_m$ . This peak is ascribed to the anti-Fano resonance between the asymmetric Kondo resonance and the zero-energy MF mode. Interestingly, in the strong-coupling regime, the Kondo-induced peak in  $L$  is shifted due to the MF-induced Zeeman splitting in the dot. For finite but small  $\epsilon_m > 0$ , the interference between two MFs restores the Kondo effect in the dot in a smaller energy scale  $\Gamma'_m$  and gives rise to an additional peak in  $L$  at  $T \sim \Gamma'_m$ , whose sign is opposite to that at  $T \sim \Gamma_m$ . In the strong-coupling regime this additional peak can cause a non-monotonic behavior of  $L$  with respect to the dot gate. Finally, we examine the case in which an ordinary spin-polarized fermion is coupled to the dot and identify the fingerprint of MFs by comparing two cases.

PACS numbers: 72.15.Jf, 73.63.Kv, 72.10.Fk

## I. INTRODUCTION

The advent of topological materials [1] has ignited a tremendous interest of the realization of quantum operations in platforms immune to decoherence processes [2]. A prominent feature of such materials is that they exhibit quasiparticle excitations similar to the elementary particles predicted by Ettore Majorana [3] and named Majorana fermions (MFs) [4–7]. In particular, the exoticness of such particles is that they coincide with their own anti-particles. The enormous interest generated by Majorana quasiparticles in solid state systems resides in the possibility of creating such excitations non-locally and manipulate them for quantum computation purposes [4]. Majorana quasiparticles behave as nonlocal qubits being resistant to decoherence phenomena. By exchanging two Majorana quasiparticles a non-trivial quantum operation (unitary transformation or braiding operation), is performed. Indeed, braiding manipulations among Majorana quasiparticles are the fundamental basis for the realization of topological quantum computation [2].

There are a plethora of proposals for the observation of Majorana quasiparticles in a diverse of solid state setups: quan-

tum Hall states,  $p$ -superconductors, or topological insulators [4, 8–12] among others. Nevertheless, the first signatures of the occurrence of such exotic excitations was reported in quasi-one-dimensional semiconductor nanowires [13]. This system consists of a nanowire with strong spin-orbit interaction put in proximity to a superconductor, and exposed to a magnetic field [14–22]. The experimental evidence of such quasiparticles [13, 23–26] was realized by means of tunnel spectroscopy. However, so far, these evidences are not totally conclusive. In these experiments, the appearance of a zero-bias anomaly (ZBA) in the nonlinear conductance is ascribed to the Majorana physics. Nevertheless, recently it has been pointed out that other sources of ZBA in normal-superconductor nanowires can occur. For instance, Kondo physics or Shiba states [27–29] or even nearly zero energy Andreev states [30, 31] and weak antilocalization [32] cannot be discarded as explanations of the observed ZBAs. Therefore, the detection of the MFs is now a dire challenge. Most of schemes for the detection up to now are exploiting the electronic transport involving the MFs. And only very recently the thermoelectric properties of Majorana fermion are examined and suggested for another way to distinguish Majorana physics from other explanations [33, 34]. Since the MF has the particle-hole symmetry itself, thermoelectric devices involving only the MF cannot generate any temperature-driven charge current nor electric-field-driven heat current. Hence,

\* minchul.lee@khu.ac.kr

an additional quantum object which breaks the particle-hole symmetry should be incorporated. The recent studies [33, 34] have coupled the MF to the simplest quantum object, that is, a spinless quantum dot (QD) and controlled the particle-hole symmetry by tuning the dot level. It turns out that the MF can give rise to a non-trivial thermoelectric response upon a thermal bias across the QD [34].

Interests for the reciprocity between heat and charge currents has been revived in systems at nanoscale [35, 36]. The electric response to a temperature gradient, in nanostructures, can achieve much bigger values in efficiency compared with macroscopic samples [37–40]. The main reason for such high heat-to-electricity conversion factors resides in the intrinsic quantum property of energy level discretization for confined systems [37]. However, in a more fundamental basis, thermoelectric transport can reveal rather useful information about the intrinsic nature of a quantum system [41–43] and about their interactions [44]. In this respect, our investigation explores the thermoelectric response to characterize the half-fermionic nature of Majorana nanowires.

In the context of the MF, mostly the spinless or spin-polarized QD is chosen because an external magnetic field is necessary for inducing the MF. However, as long as the Zeeman splitting in the QD is small enough or the external magnetic field is replaced by a proximity induced effective field due to a ferromagnetic layer, one can consider the case of the spinful QD in which the Coulomb interaction is highly relevant. In fact, the interplay of the Coulomb interaction and the MF in the Kondo dot side-coupled to a MF [see Fig. 1(a)] is found to display an interesting transport behavior [45]: The presence of the MF modifies the Kondo effect profoundly by reducing the linear conductance by a factor 3/4 or by inducing an effective Zeeman splitting on the QD, which leads to spin-split Kondo resonance.

In Ref. [45] some of the authors of this work investigated the interplay of Majorana and Kondo physics in the electrical conductance. Here, the purpose is to study the thermoelectric response of the side-coupled QD-nanowire system [see Fig. 1(a)] as a tool to detect Majorana quasiparticles. A temperature difference is established between the

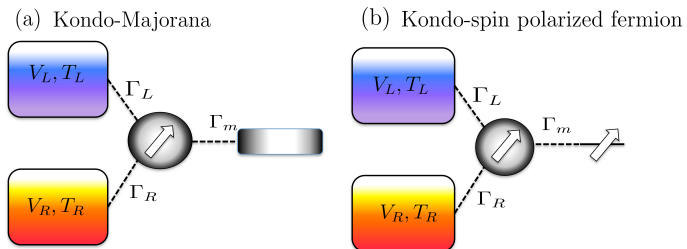


FIG. 1. (Color online) Quantum dot system coupled to two normal-metal leads (by tunneling rates  $\Gamma_{L(R)}$ ) and to (a) the MF state formed at one end of a topological superconductor wire and (b) the spin-polarized (SF) ordinary fermion state by QD-MF or QD-SF tunneling rate  $\Gamma_m$ . Due to the helical property of the MF state, only one of the spin components (say spin- $\downarrow$ ) is coupled to the MF. In the SF case, the spin is assumed to be polarized in the spin- $\downarrow$  direction.

two normal contacts coupled to the QD, then the electric response is measured. We find that thermoelectric properties in the Kondo dot-MF system depend strongly on the QD-MF coupling ( $\Gamma_m$ ), the overlap between two MF end-states ( $\epsilon_m$ ), and the Kondo temperature ( $T_K$ ). For the ideal case ( $\epsilon_m = 0$ ), due to the anti-Fano resonance between Kondo resonance peak and the zero-energy MF mode, the thermoelectrical conductance has a finite value at  $T \sim \Gamma_m$  in the weak-coupling regime ( $\Gamma_m < T_K$ ). In the strong-coupling regime ( $\Gamma_m > T_K$ ), the induced Zeeman splitting shifts the Kondo-induced peak in the thermoelectrical conductance. The finite overlap ( $0 < \epsilon_m < \Gamma_m$ ) leads to the interference between Majorana fermions and restores the Kondo effect in a small energy scale  $\Gamma'_m$  and the thermoelectrical conductance becomes finite at  $T \sim \Gamma'_m$  whose sign is opposite to that at  $T \sim \Gamma_m$ . We also consider the case in which the MF is replaced by an ordinary spin-polarized fermion (SF) and find similarities and differences between two cases, eventually identifying the fingerprint of MF in the thermoelectric effect.

In Sec. II we introduce the model of Hamiltonian employed to describe the QD-MF setup and the QD side-coupled to a spin polarized fermion. Electrical and thermoelectrical conductances are also derived in terms of the local spectral density for the interacting QD. Sec. III and IV explain our results for the temperature dependence of the electrical and thermoelectrical conductances for the QD-MF device and a comparison with the spin polarized fermion model is shown. Section V is devoted to describe our findings for the gate dependence of the thermoelectrical conductance, and we finish by enumerating the main conclusions in Sec. VI.

## II. MODEL AND METHODS

### A. Model Hamiltonian for quantum dot system side-coupled to Majorana fermion

We consider a two-terminal system in which a QD is tunnel-coupled to two normal-metal leads and to one end of a topological superconducting wire (TSW) which hosts two MFs at its ends [see Fig. 1(a)]. The on-site Coulomb repulsion in the QD is considered. The voltage bias and/or the thermal gradient will be applied across the QD. Assuming that the superconducting gap in the TSW is large enough, the effective low-energy Hamiltonian reads

$$\begin{aligned} \mathcal{H} = & \sum_{\ell\mathbf{k}\mu} \epsilon_{\mathbf{k}} c_{\ell\mathbf{k}\mu}^\dagger c_{\ell\mathbf{k}\mu} + \sum_{\ell\mathbf{k}\mu} [t_\ell d_\mu^\dagger c_{\ell\mathbf{k}\mu} + (h.c)] \\ & + \epsilon_d \sum_{\mu} n_{\mu} + U n_{\uparrow} n_{\downarrow} \\ & + 2i\epsilon_m \gamma_1 \gamma_2 + t_m (d_{\downarrow}^\dagger \gamma_1 + \gamma_1 d_{\downarrow}). \end{aligned} \quad (1)$$

Here  $c_{\ell\mathbf{k}\mu}^\dagger$  creates an electron with momentum  $\mathbf{k}$ , energy  $\epsilon_{\mathbf{k}}$ , and spin  $\mu$  in lead  $\ell = L, R$ . Two leads are assumed to share a same flat-band dispersion  $\epsilon_{\mathbf{k}}$  with a half bandwidth  $D$  and density of states  $\rho$ . The operator  $d_\mu^\dagger$  creates an electron in the single-level QD with energy  $\epsilon_d$  and spin  $\mu$ :  $n_\mu = d_\mu^\dagger d_\mu$  is

the dot occupation for spin  $\mu$ . The Coulomb repulsion in the QD is denoted by  $U$ . As mentioned in Sec. I the QD is considered to be spin degenerate [45, 46]. This condition can be achieved by using low  $g$  factor material for the QD or by using proximity with a magnetic insulator to induce the effective Zeeman splitting in the TSW [47, 48]. The tunneling between the leads and the QD is quantified by the tunneling amplitude  $t_\ell$ , which defines the tunneling rates  $\Gamma_\ell = \pi\rho|t_\ell|^2$ . For simplicity, the tunneling rates are assumed to be momentum-independent, and the total lead-QD tunneling rate is denoted as  $\Gamma = \Gamma_L + \Gamma_R$ .

The low-energy Hamiltonian of the TSW is governed by the two MF operators  $\gamma_i = \gamma_i^\dagger$  ( $i = 1, 2$ ) [49] which satisfy the Clifford algebra  $\{\gamma_i, \gamma_j\} = \delta_{ij}$ . In a finite-length TSW the two MF states have a finite overlap between their wave functions, which is quantified by the overlap integral  $\epsilon_m$ . In addition, the MF operators can be written in terms of an ordinary fermion operator  $f$  which satisfies the usual fermionic commutation relation  $\{f, f^\dagger\} = 1$  as

$$\gamma_1 = \frac{f + f^\dagger}{\sqrt{2}}, \quad \gamma_2 = \frac{f - f^\dagger}{i\sqrt{2}}. \quad (2)$$

In terms of this  $f$  operator, the Majorana coupling term in Eq. (1) can be rewritten as  $2i\epsilon_m\gamma_1\gamma_2 = \epsilon_m(f^\dagger f - 1/2)$ , which means that  $\epsilon_m$  is nothing but the energy splitting between empty ( $|0\rangle$ ) and filled ( $|1\rangle = f^\dagger|0\rangle$ ) states. We assume that the QD is coupled to the nearest MF (say  $\gamma_1$ ) and that the coupling to the other MF is negligible. The QD-MF tunneling amplitude  $t_m$  characterizes the tunneling rate  $\Gamma_m = \pi\rho_{\text{dot}}|t_m|^2$ , where  $\rho_{\text{dot}}$  is the density of states in the QD at the Fermi level. It should be noted that due to the helical property of the MF states, only one of the QD spin orientations (say spin- $\downarrow$ ) hybridizes with the MFs [45, 50, 51].

## B. Model Hamiltonian for quantum dot system side-coupled to ordinary spin-polarized fermion

In order to clarify the genuine effect by the MF it is useful to compare the MF system with the non-MF system having the same configuration. Explicitly, we replace the MF operator in Eq. (1) by an ordinary spin-polarized fermion operator  $f_\downarrow$  [see Fig. 1(b)]. In this SF case, the last line of the Hamiltonian Eq. (1) is changed into

$$\epsilon_m f_\downarrow^\dagger f_\downarrow + t_m (d_\downarrow^\dagger f_\downarrow + f_\downarrow^\dagger d_\downarrow). \quad (3)$$

In fact, the first term is effectively same as the MF coupling term (except a constant term) if  $f_\downarrow$  operator is replaced by  $f$  operator. The difference between two cases arises in the tunneling term. In the SF case, the second term in Eq. (3) represents the hopping of an electron between the QD and the SF level. In the MF case, the tunneling term

$$\frac{t_m}{\sqrt{2}} [d_\downarrow^\dagger (f + f^\dagger) + (f + f^\dagger) d_\downarrow] \quad (4)$$

includes not only the electronic hopping but also the Cooper pair creation/annihilation. This superconducting coupling should distinguish the MF case from the SF case.

## C. Linear response: electrical and thermoelectrical conductances

We are interested in measuring the charge current through the QD upon the voltage bias and/or temperature gradient between two terminals [see Fig. 1]. The current is the expectation value of the charge current operator which is given by the time derivative of the dot occupation  $\sum_\mu n_\mu$ . Using the equation-of-motion technique, the charge current can be expressed in terms of the retarded QD Green's function  $\mathcal{G}_\mu^R(t, t') = -i\Theta(t - t') \langle \{d_\mu(t), d_\mu^\dagger(t')\} \rangle$  as

$$I = \frac{4e}{h} \frac{\Gamma_L \Gamma_R}{\Gamma} \int d\epsilon (f_L(\epsilon) - f_R(\epsilon)) \sum_\mu \pi \mathcal{A}_\mu(\epsilon), \quad (5)$$

where  $f_\ell(\epsilon) = (1 + e^{(\epsilon - eV_\ell)/k_B T_\ell})^{-1}$  is the Fermi-Dirac distribution with the voltage  $V_\ell$  and the temperature  $T_\ell$  and  $\mathcal{A}_\mu(\epsilon) = -\text{Im}\mathcal{G}_\mu^R(\epsilon)/\pi$  is the QD spectral density. Assuming that the temperature gradient  $\delta T \equiv T_L - T_R$  and the voltage bias  $\delta V \equiv V_L - V_R$  across the leads are small enough, the charge current can be linearized as

$$I = G\delta V + L\delta T, \quad (6)$$

where the electrical conductance  $G$  and the thermoelectrical conductance  $L$  are given by

$$G = \frac{e^2}{h} \frac{4\Gamma_L \Gamma_R}{\Gamma} \int d\epsilon \left( -\frac{\partial f_{\text{eq}}(\epsilon)}{\partial \epsilon} \right) \sum_\mu \pi \mathcal{A}_\mu(\epsilon), \quad (7a)$$

$$L = \frac{ek_B}{h} \frac{4\Gamma_L \Gamma_R}{\Gamma} \int d\epsilon \frac{\epsilon - \epsilon_F}{k_B T} \times \left( -\frac{\partial f_{\text{eq}}(\epsilon)}{\partial \epsilon} \right) \sum_\mu \pi \mathcal{A}_\mu(\epsilon). \quad (7b)$$

Here  $f_{\text{eq}}(\epsilon)$  is the equilibrium Fermi-Dirac distribution function at the Fermi energy  $\epsilon_F$  and the background temperature  $T$ . In the low temperature limit the two linear conductances can be analytically obtained by using a Sommerfeld expansion, then

$$G \approx \frac{e^2}{h} \mathcal{T}_d(\omega)|_{\omega=\epsilon_F}, \quad (8a)$$

$$L \approx -\frac{k_B e}{h} \frac{\pi^2 k_B T}{3} \left. \frac{\partial_\omega \mathcal{T}_d(\omega)}{\mathcal{T}_d(\omega)} \right|_{\omega=\epsilon_F}, \quad (8b)$$

where  $\mathcal{T}_d(\omega) = (4\Gamma_L \Gamma_R / \Gamma) \sum_\mu \pi \mathcal{A}_\mu(\omega)$  is the dot transmission. It should be noted that  $L$  becomes finite only if the spectral density is asymmetric with respect to the Fermi level: if the spectral density has larger weight at  $|\omega| \sim T$  in the particle (hole) part than in the hole (particle) part,  $L$  (in unit of  $k_B e/h$ ) becomes positive (negative) at temperature  $T$ .

## D. NRG and Kondo regime

The NRG method [52, 53] is known to be highly effective in studying the effect of the strong Coulomb interaction non-perturbatively. We have already used the NRG technique for

investigating the electric property of our system in Ref. [45], finding very interesting interplay between the Majorana and Kondo physics. For a full review of the NRG, one can refer to Ref. [54]. Below we give a brief introduction of the NRG used in this work.

The NRG method consists in a series of consecutive exact diagonalizations of an appropriately discretized form of  $\mathcal{H}$  represented by a linear tight-binding chain. In each partial diagonalization step the spectrum is truncated by retaining only those low-energy excitations that contains the strongest coupling terms. Better improvements of the NRG approach such as the density-matrix NRG [55], the  $z$ -averaging, and refinement of the logarithmic discretization [56, 57] allows us to calculate the dynamical properties at higher energies in a reliable and rather accurate way, which is essential for our thermoelectric study. The NRG procedure also exploits the existence of symmetries for better efficiency. Note that this system has two conserved quantities:  $[Q_\uparrow, \mathcal{H}] = [P_\downarrow, \mathcal{H}] = 0$  where  $Q_\uparrow$  and  $P_\downarrow$  are charge number operator for spin- $\uparrow$  electrons and parity operator for the sum  $Q_\downarrow$  of spin- $\downarrow$  electrons and  $f$  electrons, respectively. Note that the QD-MFS hopping changes  $Q_\downarrow$  by even numbers only. To obtain the electrical conductance  $G$  and the thermoelectrical conductance  $L$ , at each iteration in the backward stage, the spin-resolved QD spectral density  $A_\mu(\epsilon)$  is calculated

$$A_\mu^{(N)}(\epsilon) = \sum_{nm} \langle n | d_\sigma^\dagger | m \rangle_N \langle m | d_\sigma \rho_N^{\text{red}} + \rho_N^{\text{red}} d_\sigma | n \rangle_N \times \delta[\epsilon - (E_n^{(N)} - E_m^{(N)})], \quad (9)$$

where  $|n\rangle_N$  and  $E_n^{(N)}$  are the eigenstates and the corresponding eigenenergies obtained at iteration  $N$ . The reduced density matrix  $\rho_N^{\text{red}}$  is iteratively calculated in backward process, starting at the final iteration  $M$  which is determined by the condition that  $T \sim T_M$  where  $T_M$  is the energy scale corresponding to iteration  $M$ . At the final iteration, the reduced matrix is given by [54, 55, 58]

$$\rho_M^{\text{red}} = \sum_n \frac{e^{-\beta E_n^{(M)}}}{Z_M} |n\rangle_M \langle n| \quad \text{with} \quad Z_M = \sum_n e^{-\beta E_n^{(M)}}. \quad (10)$$

Since we are interested in the Kondo regime, throughout our work, we have used the following values of the parameters unless specified otherwise:  $\epsilon_d = -0.2D$ ,  $U = D$ , and  $\Gamma = 0.04D$  using the bandwidth  $D$  as the energy unit ( $D = 1$ ).

### III. LONG TSW CASE: $\epsilon_m = 0$

For an ideal TSW the two MF end states have zero overlap. The parameter that quantifies the degree of overlap between the two end states is denoted by  $\epsilon_m$  that is considered null through this section. Here, we present our NRG results for both electrical and thermoelectrical conductances in this case. Indeed, the electric response in the QD-MF setup was discussed in Ref. [45], however for completeness we briefly explain the main findings for the electrical conductance and

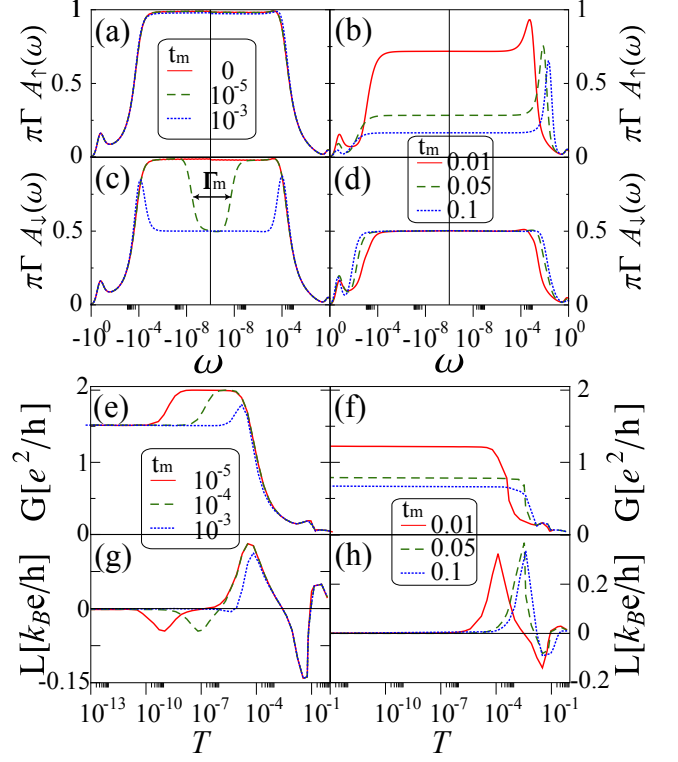


FIG. 2. (Color online) Dynamical and electric/thermoelectric transport features in the MF case for  $\epsilon_m = 0$ . Left and right panels correspond to the weak- ( $\Gamma_m < T_K$ ) and strong-coupling ( $\Gamma_m > T_K$ ) regimes, respectively: [(a),(b)] QD spin- $\uparrow$  spectral density, [(c),(d)] QD spin- $\downarrow$  spectral density, [(e),(f)] electrical conductance, and [(g),(h)] thermoelectrical conductance for annotated values of  $t_m$ . Here we have used  $\delta = 0.8$  ( $\epsilon_d = -0.2$  and  $U = 1$ ) and  $\Gamma = 0.04$ .  $T_K = 2.64 \times 10^{-4}$  with these parameters.

discuss in detail the thermoelectrical response of our device. Importantly, as we discuss below,  $L$  exhibits different behaviors for the weak- ( $\Gamma_m < T_K$ ) and strong- ( $\Gamma_m > T_K$ ) coupling regimes.

#### A. Weak-coupling regime, $\Gamma_m < T_K$

First, we investigate the weak-coupling regime ( $\Gamma_m < T_K$ ) [see the left panels of Fig. 2]. When the QD is uncoupled from the TSW, i.e., when  $t_m = 0$ , the QD spin-resolved spectral densities  $A_\mu(\omega)$  [see Fig. 2(a) and 2(c)] exhibit a Kondo resonance peak located at  $\omega = 0$  with a half-width  $T_K$  and two side resonance peaks at  $\omega \approx \epsilon_d, \epsilon_d + U$ . For a finite but weak QD-MF coupling ( $t_m > 0$ ), while  $A_\uparrow(\omega)$  is not affected by the coupling to the MF since the spin  $\uparrow$  is not directly coupled to the MF [see Fig. 2(a) and 2(c), for  $t_m = 0, 10^{-3}, 10^{-5}$ ],  $A_\downarrow(\omega)$  exhibits a half-dip whose width is comparable to  $\Gamma_m$  [see Fig. 2(c)]. The half-fermionic dip is ascribed to the destructive interference between the Kondo resonance and the MF states. As a result an anti-Fano resonance occurs due to the half-fermionic nature of the MF state [45, 59]. The resultant linear conductance  $G$  as a function of

the temperature is shown in Fig. 2(e). At low temperatures ( $T < \Gamma_m$ ),  $G = e^2/h + e^2/2h = 3e^2/2h$ , owing to the half-fermionic anti-Fano resonance. For larger temperature ( $\Gamma_m < T < T_K$ ) the conductance restores the Kondo unitary-limit value,  $2e^2/h$ , eventually decreasing to 0 for  $T_K < T$  because of the Coulomb blockade and the destruction of the Kondo effect.

The thermoelectrical conductance  $L$  displays more interesting features as shown in Fig. 2(g). Before addressing the thermoelectric effect ascribed to the Majorana physics, we first need to understand the behavior of  $L$  due to the Kondo effect itself. In the symmetric case, when  $\delta = 0$ , with  $\delta = 2\epsilon_d + U$  electron-hole symmetry holds and the thermoelectrical conductance vanishes completely. Away from this special situation ( $\delta \neq 0$ ) the Kondo resonance peak in  $A_\mu(\omega)$  is always asymmetric: the Kondo peak is slightly shifted toward the positive (negative) frequency part for  $\delta > 0$  ( $\delta < 0$ ), which leads to a positive (negative) peak in  $L$  at  $T \sim T_K$  [60, 61]: As shown in Fig. 2(g)  $L$  has a positive peak at  $T \sim T_K \sim 10^{-4}$  since  $\delta > 0$ . This asymmetry can be understood in terms of the slope of the spectral density at the Fermi level  $\epsilon_F$ . From the Luttinger theorem [62], the derivative of the spectral density is given by

$$\left. \frac{\partial A_\mu(\epsilon)}{\partial \epsilon} \right|_{\epsilon=\epsilon_F} = \frac{\sin(2\langle n_\mu \rangle \pi) \sin^2(\langle n_\mu \rangle \pi)}{\pi z_\mu \Gamma^2}, \quad (11)$$

where  $z_\mu = 1/(1 - \partial_\epsilon \Sigma_\mu^R(\epsilon_F))$ ,  $\Sigma_\mu^R$  is the real part of the retarded self-energy per spin and  $\langle n_\mu \rangle$  is the dot occupation per spin. For  $\delta > 0$  ( $\delta < 0$ ),  $\langle n_\mu \rangle$  is less (larger) than  $1/2$  so the derivative becomes positive (negative) and, accordingly, the Kondo resonance is slightly shifted toward the positive (negative) frequency. At larger frequencies, the side peaks in  $A_\mu(\omega)$  are responsible for the two peaks in  $L$  at  $T \sim |\epsilon_d|$  and  $|\epsilon_d + U|$  whose signs are opposite. Hence, in the Kondo regime,  $L$  experiences two sign changes as  $T$  increases from  $T_K$  to high temperatures as predicted in Ref. [60] and reproduced in our calculations.

In the presence of the MF, on the other hand, an additional peak, whose sign is opposite to that of the Kondo-induced peak, occurs at  $T \sim \Gamma_m < T_K$ . It is surely due to the particle-hole asymmetry of the half-dip in  $A_\downarrow(\omega)$  whose width is  $\Gamma_m$  [see Fig. 2(c)]. This asymmetry also originates from that of the Kondo resonance peak. The destructive interference responsible for the dip is stronger at the frequency side in which the Kondo peak is located. As a result, the dip is also slightly shifted toward the same frequency side as the Kondo peak, leading to the asymmetry of the dip in the spectral density and the observed peak in  $L$ . As  $t_m$  increases, the half-dip is widened and eventually trims the Kondo resonance peak when the dip width is comparable to the Kondo peak width [see Fig. 2(c)]. Hence, the MF-induced peak in  $L$  disappears when  $\Gamma_m \sim T_K$ .

### B. Strong-coupling regime, $\Gamma_m > T_K$

In the strong-coupling regime, the Kondo effect still survives but is modified as follows: First, the Kondo peak in

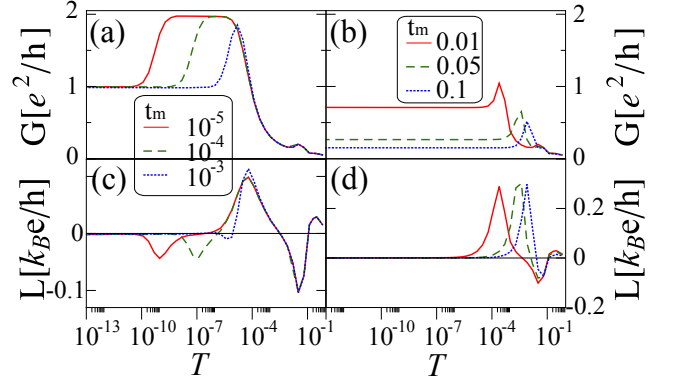


FIG. 3. (Color online) Electric/thermoelectric transport features in the SF case for  $\epsilon_m = 0$ . Left and right panels correspond to the weak- ( $\Gamma_m < T_K$ ) and strong-coupling ( $\Gamma_m > T_K$ ) regimes, respectively: [(a),(b)] electrical conductance and [(c),(d)] thermoelectrical conductance for annotated values of  $t_m$ . Here we have used the same values of the parameters as in Fig. 2.

$A_\uparrow(\omega)$  shifts with increasing  $t_m$  [see Fig. 2(b)]. The peak moves toward positive (negative) frequencies for  $\delta > 0$  ( $\delta < 0$ ). It is attributed to the induced Zeeman splitting  $\Delta_Z$  caused by the Coulomb interaction and the broken time-reversal symmetry in the TSW [45]. While its unnormalized value for  $t_m \ll |\epsilon_d|$ ,  $\epsilon + U$  is given by

$$\Delta_Z^{(0)} = -\frac{t_m^2}{2} \frac{\delta}{(\epsilon_m + \delta - \epsilon_d)(\epsilon_m - \epsilon_d)} \quad (12)$$

for a general value of  $\epsilon_m$ , in fact the renormalization due to the coupling to the leads makes it larger than  $\Delta_Z^{(0)}$  in magnitude [45]. On the other hand,  $A_\downarrow(\omega)$  is not affected by the induced Zeeman splitting because it is directly coupled to the zero-energy MF and pinned to the Fermi level. The height of  $\pi\Gamma A_\downarrow(\omega)$  is fixed at  $1/2$  [see Fig. 2(d)]. Since the Kondo peak in  $A_\uparrow(\omega)$  is shifted, the linear conductance at low temperatures is smaller than the weak-coupling-limit value,  $3e^2/2h$  and decreases to  $e^2/2h$  as  $t_m$  increases [see Fig. 2(f)].

The effect of the QD-MF coupling in the thermoelectrical conductance is the shift of the Kondo-induced peak in  $L$  with increasing  $t_m$  [see Fig. 2(h)]. The shift is obviously due to that of the Kondo peak in  $A_\uparrow(\omega)$  by the induced Zeeman splitting explained above. Hence, the position of the Kondo-induced peak in  $L$  should follow the induced Zeeman splitting:  $T \sim \Delta_Z$ .

### C. SF case

Now one should ask whether the observed MF-induced features in  $L$  are the genuine effects of the Majorana physics or not. For that purpose, we have repeated the same calculations by using the Hamiltonian, Eq. (3) with a zero-energy spin-polarized level ( $\epsilon_m = 0$ ). First, we have obtained the qualitatively same spectral densities as in the MF case:  $A_\uparrow(\omega)$  features the Kondo resonance peak at  $\omega = 0$  in the weak-



coupling regime and its peak moves due to the effective Zeeman splitting in the strong-coupling regime.  $A_{\downarrow}(\omega)$  also exhibits the dip structure due to the anti-Fano resonance by the side-coupled spin-polarized level. One and only difference between two cases is that the dip in the SF case is a full dip so that  $A_{\downarrow}(\omega = 0) = 0$ . As a result, the low-temperature value of the linear conductance, which is  $e^2/h$  in the weak-coupling regime, is decreased compared to the MF case [see Figs. 3(a) and 3(b)]. However, the other features of the linear conductance is the same as those in the MF case. The thermoelectrical conductance also exhibits the same qualitative behavior as that of the MF case [see Figs. 2(c) and 2(d)]: the appearance of the MF-induced peak at  $T \sim \Gamma_m$  in the weak-coupling regime and the shift of the Kondo-induced peak at  $T \sim \Delta_Z$  in the strong-coupling regime. Hence, for  $\epsilon_m = 0$ , while the two cases exhibit different behaviors of the electrical conductance, the measurement of the thermoelectrical conductance cannot distinguish the MF state from the ordinary spin-polarized state.

#### IV. SHORT TSW CASE: $\epsilon_m \neq 0$

The overlap between Majorana states depends on the relative length between the TSW length and the localization length of the Majorana states. Hence, by changing the relative length (for example, the TSW length by tuning the position-dependent gate potential or the MF localization length by controlling the superconducting gap and/or the gate potential), the overlap amplitude  $\epsilon_m$  can be varied. Similarly, the level of the ordinary spin-polarized state can be tuned by electric or magnetic methods. In this section, we examine whether the MF can display a genuine thermoelectric effect for finite  $\epsilon_m$ , which cannot be reproduced by the SF level.

##### A. Weak-coupling regime, $\Gamma_m < T_K$

The left panels of Fig. 4 show the QD spectral densities, the linear conductance, and the thermoelectrical conductance in the weak-coupling regime for  $\epsilon_m \neq 0$ . As for  $\epsilon_m = 0$ , the Kondo peak in  $A_{\uparrow}(\omega)$  remains intact irrespectively of the value of  $\epsilon_m$  [see Fig. 4(a)]. An interesting change occurs in  $A_{\downarrow}(\omega)$ : Inside the half-dip, a central peak is developed for finite values of  $\epsilon_m$  [see Fig. 4(c)], which originates from the interference between the MFs,  $\gamma_1$  and  $\gamma_2$ . Finite coupling  $2\epsilon_m$  between  $\gamma_1$  and  $\gamma_2$  broadens the  $\gamma_2$  spectral density with the width  $\Gamma'_m \approx (2\epsilon_m)^2/\Gamma_m$  and in turn the scattering from the resonance level of  $\gamma_2$  results in the destructive interference for  $\gamma_1$ , forming a full dip in the  $\gamma_1$  spectral density. Hence, inside the dip, the anti-Fano resonance which suppressed the Kondo effect does not happen any longer since  $\gamma_1$  which would interfere with the QD spin has no excitation in that range of energy, and the Kondo effect is restored. As  $\epsilon_m$  increases, the central peak gets wider and the full Kondo resonance peak is restored when  $\Gamma'_m \sim \Gamma_m$  or  $\epsilon_m \sim \Gamma_m$ . The restoration of the Kondo effect at low frequencies is well reflected in the linear conductance for  $T < \Gamma'_m$  [see Fig. 4(e)].

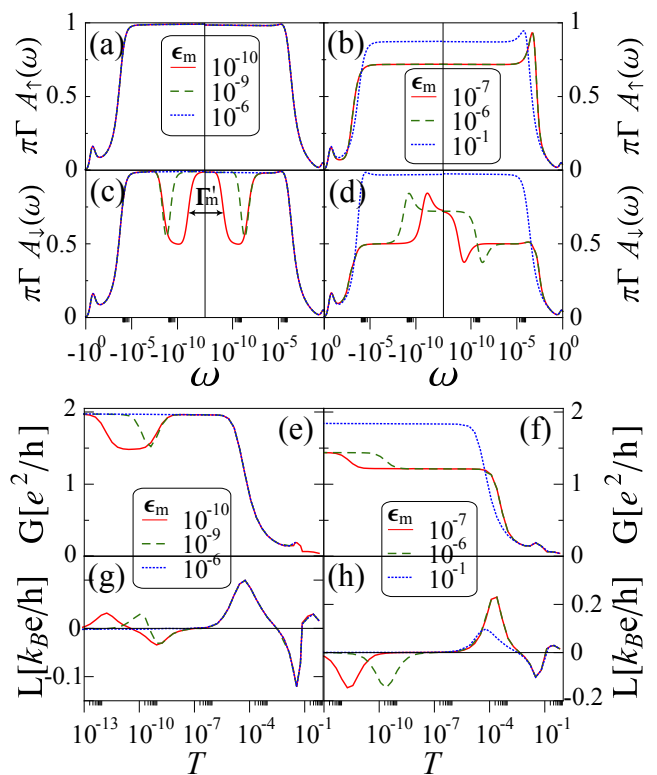


FIG. 4. (Color online) Spin-resolved spectral densities and electric/thermoelectric conductances in the MF case for  $\epsilon_m \neq 0$ . Left and right panels correspond to the weak- ( $t_m = 10^{-5}$ ) and strong-coupling ( $t_m = 10^{-2}$ ) regimes, respectively: [(a),(b)] QD spin- $\uparrow$  spectral density, [(c),(d)] QD spin- $\downarrow$  spectral density, [(e),(f)] electrical conductance, and [(g),(h)] thermoelectrical conductance for annotated values of  $\epsilon_m$ . Here we have used the same values of the parameters as in Fig. 2.

The central peak in  $A_{\downarrow}(\omega)$  due to the restoration of the Kondo effect also has its trace on the thermoelectrical conductance. Figure 4(g) shows that an additional peak in  $L$  at  $T \sim \Gamma'_m$  is formed on top of  $L$  in the  $\epsilon_m = 0$  case. In fact, the central peak is also asymmetric like the original Kondo peak. It should be noted that the dip in the  $\gamma_1$  spectral density is symmetric since the MF always maintains the particle-hole symmetry. So, the asymmetry of the central peak has the same origin as the Kondo peak, and the signs of the Kondo-induced peak and the finite- $\epsilon_m$ -induced peak in  $L$  are always same. As  $\epsilon_m$  increases up to  $\sim \Gamma_m$ , the half-dip and the inner central peak in  $A_{\downarrow}(\omega)$  cancels out each other. Therefore, the two MF-related peaks are merged and disappear completely when  $\epsilon_m \sim \Gamma_m$ , making  $L \approx 0$  for  $T \ll T_K$ .

##### B. Strong-coupling regime, $\Gamma_m > T_K$

In the strong-coupling regime the finite  $\epsilon_m$  removes the half-fermionic Fano resonance at the Fermi level. As a result,  $\pi\Gamma A_{\downarrow}(\omega)$ , which was pinned to  $1/2$  at  $\omega = 0$  for  $\epsilon_m = 0$ , becomes larger than  $1/2$ , restoring the Kondo correlation a bit

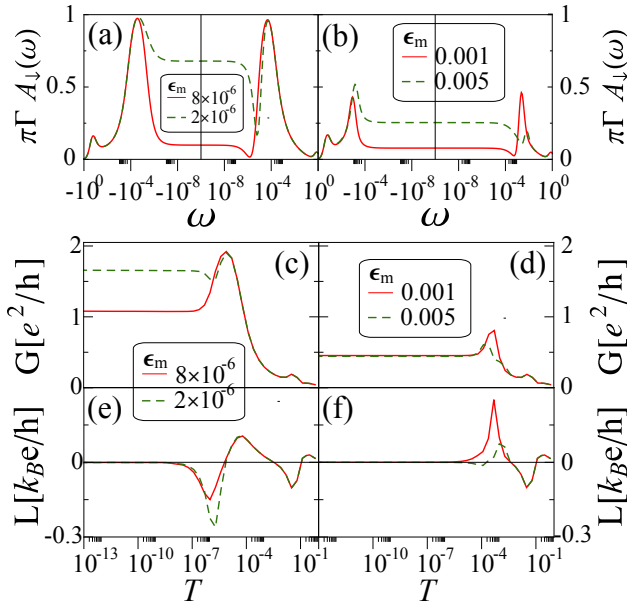


FIG. 5. (Color online) Dynamical and electric/thermoelectric transport features in the SF case for  $\epsilon_m > 0$ . Left and right panels correspond to the weak- ( $t_m = 5 \times 10^{-4}$ ) and strong-coupling ( $t_m = 10^{-2}$ ) regimes, respectively: [(a),(b)] QD spin- $\downarrow$  spectral density, [(c),(d)] electrical conductance, and [(e),(f)] thermoelectrical conductance for annotated values of  $\epsilon_m$ . Here we have used the same values of the parameters as in Fig. 2.

[see Fig. 4(d)]. Instead, since the MF states are now energy-split, the half-value pinning is retained in  $\Gamma'_m < |\omega| < \Gamma_m$  for  $\epsilon_m < \Gamma_m$ . In the frequency windows  $|\omega| < \Gamma'_m$  we observe in  $A_\downarrow(\omega)$  an asymmetric peak (with a small dip in the opposite side) whose position is approximately at  $\omega \approx -\text{sgn}(\delta)\Gamma_m/\pi$ . The peak in  $A_\downarrow(\omega)$  is located in the opposite side with respect to the Zeeman-splitting peak in  $A_\uparrow(\omega)$  [see Fig. 4(b)]. We speculate that the asymmetric peak in  $A_\downarrow(\omega)$  is the outcome of the competition between the induced Zeeman splitting on spin  $\downarrow$  (so the peak would appear at  $\omega \approx -\Delta_Z$ ) and the half-fermionic pinning at the energy-split MF level. Note that this central peak has the opposite asymmetry with respect to that in the weak-coupling regime. Hence, due to this asymmetric peak structure, an additional peak in  $L$  arises at  $T \sim \Gamma'_m$ , whose sign is opposite to that of the Kondo-induced peak [see Fig. 4(h)]. Finally, owing to the increase in  $A_\downarrow(\omega)$  at low frequencies, the low-temperature value of the linear conductance  $G$  increases a bit [see Fig. 4(f)].

For  $\epsilon_m \gg \Gamma_m$ , the MF levels which are at  $\pm\epsilon_m$  do not interfere with the Kondo resonant level any longer so that the Kondo physics in the QD is completely revived [45]: The peak in  $L$  at  $T \sim \Gamma'_m$  disappears.

### C. SF case

It is obvious that the additional low-temperature features in  $L$  of the MF case with finite  $\epsilon_m$  cannot be reconstructed by the SF case with zero  $\epsilon_m$ . For the SF case, the effect of  $\epsilon_m$

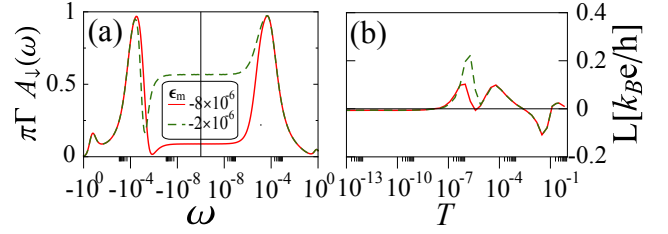


FIG. 6. (Color online) (a) QD spin- $\downarrow$  spectral density and (b) thermoelectrical conductance in the SF case for  $\epsilon_m < 0$  in the weak-coupling case. The corresponding values of  $\epsilon_m$  are annotated. Here we use the same values of parameters as in the weak-coupling regime of Fig. 5.

being finite on the QD spectral density is quite simple.  $A_\uparrow(\omega)$  is not so affected as long as  $|\epsilon_m| < \Gamma_m$ , and the full dip in  $A_\downarrow(\omega)$  due to the anti-Fano resonance by the spin-polarized level is formed at  $\omega = \epsilon_m/\hbar$  [see Figs. 5(a), 5(b) and 6(a)]. The only difference between the weak- and strong-coupling regimes is whether the dip is so narrow as to be confined inside the Kondo resonance peak or wide enough to suppress it. Hence, the electrical and thermoelectrical conductances are qualitatively similar to those in the  $\epsilon_m = 0$  case: compare Figs. 3(a-d) and 5(c-f), respectively. Note that for  $\epsilon_m \neq 0$  and in the weak-coupling regime the SF-induced peak in  $L$  is formed at  $T \sim \epsilon_m$ . For  $\epsilon_m < 0$ , the dip moves toward the negative frequency [see Fig. 6(a)] so that the sign of the SF-induced peak is reversed [see Fig. 6(b)].

Therefore, as reflected in Figs. 5 and 6, the SF case with finite  $\epsilon_m$  cannot reproduce the temperature dependence of  $L$  in the MF case with finite  $\epsilon_m$ . Hence, the observed features of  $L$  in the MF case are genuine effects only the MF can generate. The reason why the MF and SF cases become distinguishable from each other for  $\epsilon_m \neq 0$  is that the MF state is particle-hole symmetric while the SF state is not. In the MF case the only source of the asymmetry is the Kondo effect while in the SF case the SF level can also make the system asymmetric. For  $\epsilon_m = 0$  this difference did not show up since the levels are at the Fermi level and particle-hole symmetric.

## V. GATE DEPENDENCE OF THE THERMOELECTRICAL CONDUCTANCE

In the previous sections it is shown that the MF adds additional peaks to the temperature dependence of  $L$ . Since the MF is particle-hole symmetric, the finite  $L$  is attributed to the asymmetry of the Kondo resonance peak, or in other words, nonzero  $\delta$ . Therefore, by tuning the value of  $\delta$  or the gate voltage on the QD, the magnitude and the sign of  $L$  can be controlled. In this section we investigate the gate dependence of  $L$  in the Kondo regime.

Before addressing the weak- and strong-coupling regimes separately, we discuss the common features seen in both cases. As shown in Figs. 7 and 8, the thermoelectrical conductance vanishes at  $\delta = 0$ , irrespectively of the values of the other parameters. It is because at  $\delta = 0$  the whole system is particle-

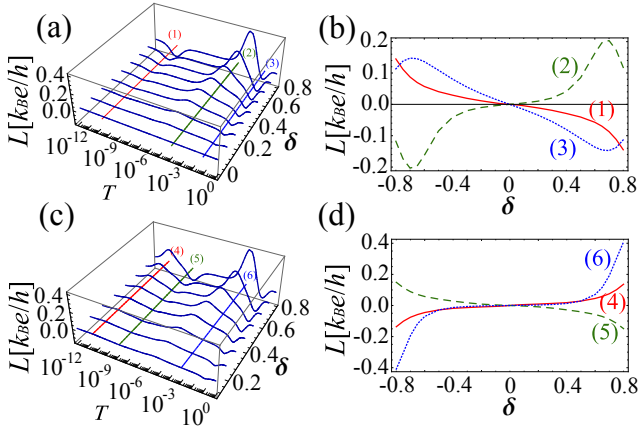


FIG. 7. (Color online) Gate dependence of  $L$  in the weak-coupling regime for [(a),(b)] long TSW case ( $\epsilon_m = 0$  and  $t_m = 10^{-6}$ ) and [(c),(d)] short TSW case ( $\epsilon_m = 10^{-10}$  and  $t_m = 10^{-5}$ ). In (b) and (d) the thermoelectrical conductances  $L$  are drawn as functions of  $\delta$  at fixed temperatures, or along the straight lines in (a) and (c), respectively: (1) MF-induced peak ( $T = 3.0 \times 10^{-11}$ ), (2) Kondo-induced peak ( $T = 1.3 \times 10^{-4}$ ), (3) charge-fluctuation-induced peak ( $T = 6.4 \times 10^{-2}$ ), (4) restored-Kondo-induced peak ( $T = 3.7 \times 10^{-12}$ ), (5) MF-induced peak ( $T = 1.9 \times 10^{-9}$ ), and (6) Kondo-induced peak ( $T = 1.0 \times 10^{-3}$ ).

hole symmetric even with nonzero  $\epsilon_m$ . In addition,  $L$  is always odd function upon  $\delta \rightarrow -\delta$ . It is attributed to the fact that the MF is particle-hole symmetric and the QD is the only source for the asymmetry. Therefore, as the temperature (and other parameters) changes, the sign of  $L$  changes globally as observed in the non-interacting case [34].

#### A. Weak-coupling regime, $\Gamma_m < T_k$

Figure 7 shows the thermoelectrical conductance as a function of the temperature  $T$  and the asymmetry parameter  $\delta$  (or the QD level) in the weak-coupling regime of both the  $\epsilon_m = 0$  and  $\epsilon_m \neq 0$  cases. The main qualitative features of the temperature dependence of  $L$  observed in the previous sections do not change with  $\delta$ , as seen in Figs. 7(a) and 7(c). Instead, the position and height of the peaks are gradually changed. Owing to the dependence of the Kondo temperature on the QD level, the Kondo-induced peaks [see curves (2) and (6) in Fig. 7] move toward the larger temperature as  $|\delta|$  increases. However, the MF-related peaks, that is, the MF-induced and restored-Kondo-induced peaks [see curves (1), (4) and (5) in Fig. 7] do not move so much upon changing  $\delta$  since  $\Gamma_m$  and  $\Gamma'_m$  are quite immune to the QD level in the weak-coupling regime [see Figs. 7(a) and 7(c)]. The heights of the peaks usually increase with increasing  $|\delta|$  [see Figs. 7(b) and 7(d)]. It is because the asymmetry is the larger for the larger  $|\delta|$ .

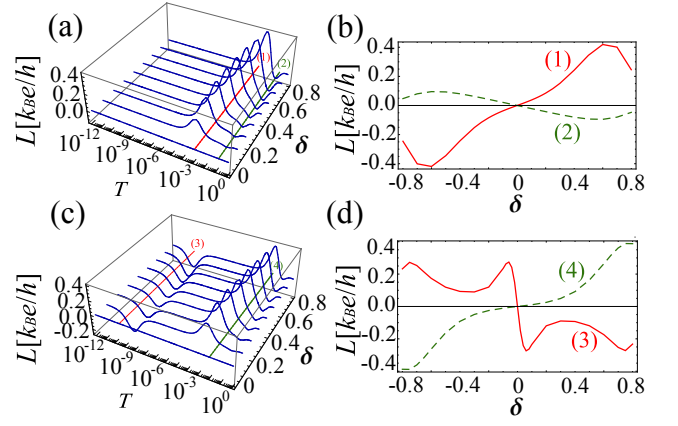


FIG. 8. (Color online) Gate dependence of  $L$  in the strong-coupling regime for [(a),(b)] long TSW case ( $\epsilon_m = 0$  and  $t_m = 0.02$ ) and [(c),(d)] short TSW case ( $\epsilon_m = 10^{-6}$  and  $t_m = 0.05$ ). In (b) and (d) the thermoelectrical conductances  $L$  are drawn as functions of  $\delta$  at fixed temperatures, or along the straight lines in (a) and (c), respectively: (1) Zeeman-splitting-induced peak ( $T = 1.0 \times 10^{-3}$ ), (2) charge-fluctuation-induced peak ( $T = 1.3 \times 10^{-1}$ ), (3) restored-Kondo-induced peak ( $T = 3.0 \times 10^{-11}$ ), and (4) Zeeman-splitting-induced peak ( $T = 8.0 \times 10^{-3}$ ).

#### B. Strong-coupling regime, $\Gamma_m > T_k$

Finally, we consider the gate dependence of the thermoelectrical conductance in the strong-coupling regime. As in the weak-coupling regime, the main features of  $L$  discussed before are present for all values of  $\delta$ , as can be seen in Fig. 8. For  $\epsilon_m = 0$  [see Figs. 8(a) and 8(b)], the gate dependence of  $L$  in strong coupling regime has similar behavior with the weak-coupling regime: compare (2) and (3) in Fig. 7(b) with (1) and (2) in Fig. 8(b), respectively.  $L$  increases with  $|\delta|$ . For  $\epsilon_m \neq 0$  [see Figs. 8(c) and 8(d)], on the other hand, one can observe a non-monotonic behavior of  $L$  with respect to  $\delta$  [see (3) in Fig. 8(d)]. In fact, the peak due to the restored Kondo effect is shifted as  $\delta$  is varied [see Fig. 8(c)]: the peak first moves toward higher temperature as  $|\delta|$  increases from zero and at some value of  $|\delta|$  the shift is reversed, returning back as  $|\delta|$  approaches  $U$ , while the change in the peak position is within the order of magnitude  $\sim \Gamma'_m$ . This shift of the peak results in the observed non-monotonic behavior of  $L$  at a fixed temperature. Surely, in the strong-coupling regime, the Majorana hybridization  $\Gamma'_m$  should be renormalized depending on the value of  $\epsilon_d$ . While it is not easy to quantify the renormalization, there is an intuitive way to understand the non-monotonic behavior: The restore Kondo peak in  $A_\downarrow$  in the strong-coupling regime [see Fig. 4(d)] is related to the induced Zeeman splitting  $\Delta_Z$  acting on the spin  $\downarrow$ , as mentioned before. For small  $|\delta|$ ,  $\Delta_Z$  is also small [see Eq. (12)] such that  $\Delta_Z < \Gamma'_m$ . In this case, the peak follows the induced Zeeman splitting  $\Delta_Z$ , explaining the initial increase of the peak position. However, once  $\Delta_Z$  exceeds  $\Gamma'_m$ , the pinning by the MFs prevents the peak from moving toward higher temperature further. Instead, as  $|\delta|$  increases, the QD density of states  $\rho_{\text{dot}}$  increases due to the resonance levels, and accordingly  $\Gamma'_m$  de-



creases (note that  $\Gamma'_m \propto 1/\Gamma_m \propto 1/\rho_{\text{dot}}$ ). Hence, the peak in  $A_{\downarrow}$  moves toward lower temperature. This non-monotonic behavior of  $L$  is the outcome of the interplay between the Kondo and Majorana physics so its experimental observation can be much stronger evidence of the existence of the MFs.

## VI. CONCLUSION

We have investigated the thermoelectric properties of strongly correlated quantum dot side-coupled to the Majorana fermions. The electrical conductance  $G$  and the thermoelectrical conductance  $L$  through QD are calculated using the numerical renormalization group method in both weak- and strong-coupling regimes. The side-coupled Majorana fermion causes the anti-Fano resonance in weak-coupling regime and the induced Zeeman splitting in strong-coupling regime. These two effects considerably modify the shape of

the Kondo resonance peak in the QD spectral densities and eventually transform the structure of  $L$  and  $G$ . Especially, with a finite overlap between MFs ( $\epsilon_m \neq 0$ ), the thermoelectrical conductance  $L$  exhibits conspicuous characteristics – additional peaks in  $L$  and the non-monotonic dependence of  $L$  on the gate voltage – which cannot be attained by an ordinary fermion. We expect that our work can act as a guide for finding the unique signal of Majorana fermion in thermoelectric devices.

## ACKNOWLEDGMENTS

This work was supported by MINECO Grant No. FIS2011-23526, in part by the Kavli Institute for Theoretical Physics through NSF grant PHY11-25915, and by the National Research Foundation of Korea (NRF) grants funded by the Korea government (MSIP) (No. 2011-0030046).

- 
- [1] M. Z. Hasan, and C. L. Kane, *Rev. of Mod. Phys.* **82**, 3045 (2010).
  - [2] C. Nayak, S. H. Simon, A. Stern, M. Freedman, and S. Das Sarma, *Rev. Mod. Phys.* **80**, 1083 (2008).
  - [3] E. Majorana, *Nuovo Cimento* **14**, 171 (1937).
  - [4] A. Y. Kitaev, *Physics Uspekhi* **44**, 131 (2001).
  - [5] F. Wilczek, *Nat. Phys.* **5**, 614 (2009).
  - [6] J. Alicea, *Rep. Prog. Phys.* **75**, 076501 (2012)
  - [7] C. W. J. Beenakker, *Annual Review of Condensed Matter Physics* **4** 113 (2013).
  - [8] G. Moore and N. Read, *Nucl. Phys. B* **360**, 362 (1991).
  - [9] D. A. Ivanov, *Phys. Rev. Lett.* **86**, 268 (2001).
  - [10] S. Das Sarma, C. Nayak, and S. Tewari, *Phys. Rev. B* **73**, 220502 (2006).
  - [11] L. Fu, and C. L. Kane, *Phys. Rev. Lett.* **100**, 096407 (2012).
  - [12] J. Linder, Y. Tanaka, K. Yokoyama, A. Sudbø, and N. Nagaosa, *Phys. Rev. Lett.* **104**, 067001 (2010).
  - [13] V. Mourik, K. Zuo, S. M. Frolov, S. R. Plissard, E. P. A. M. Bakkers, and L. P. Kouwenhoven, *Science* **336**, 1003 (2012).
  - [14] Y. Oreg, G. Refael, and F. von Oppen, *Phys. Rev. Lett.* **105**, 177002 (2010).
  - [15] J. Alicea, *Phys. Rev. B* **81**, 125318 (2010).
  - [16] R. M. Lutchyn, J. D. Sau, and S. Das Sarma, *Phys. Rev. Lett.* **105**, 077001 (2010).
  - [17] J. Linder and A. Sudbø, *Phys. Rev. B* **82**, 085314 (2010).
  - [18] A. C. Potter, and P. A. Lee, *Phys. Rev. B* **83**, 184520 (2011).
  - [19] J. Liu, A. C. Potter, K. T. Law, and P. A. Lee, *Phys. Rev. Lett.* **109**, 267002 (2012).
  - [20] F. Pientka, G. Kells, A. Romito, P. W. Brouwer, and F. von Oppen, *Phys. Rev. Lett.* **109**, 227006 (2012).
  - [21] E. Prada, P. San-Jose, R. Aguado, *Phys. Rev. B* **86**, 180503(R) (2012).
  - [22] J. S. Lim, R. López, and L. Serra, *New J. Phys.* **14**, 083020 (2012).
  - [23] M. T. Deng, C. L. Yu, G. Y. Huang, M. Larsson, P. Cardoff, and H. Q. Xu, *Nano Lett.* **12**, 6414 (2012).
  - [24] A. Das, Y. Ronen, Y. Most, Y. Oreg, M. Heinblum, and H. Shtrikman, *Nat. Phys.* **8**, 887 (2012).
  - [25] H. O. H. Churchill, V. Fatemi, K. Grove-Rasmussen, M. T. Deng, P. Caroff, H. Q. XU, and C. M. Marcus, *Phys. Rev. B* **87**, 241401 (2012).
  - [26] A. D. K. Finck, D. J. van Harlingen, P. K. Mohseni, K. Jung, and X. li, *Phys. Rev. Lett.* **110**, 126406 (2013).
  - [27] W. Chang, V. E. Manucharyan, T. S. Jespersen, J. Nygård, and C. M. Marcus, *Phys. Rev. Lett.* **110**, 217005 (2013).
  - [28] E. J. H. Lee, X. Jiang, R. Aguado, G. Katsaros, C. M. Lieber, and S. De Franceschi, *Phys. Rev. Lett.* **109**, 186802 (2012).
  - [29] R. Žitko, J. S. Lim, R. Lopez, and R. Aguado, arXiv:1405.6084 (2014).
  - [30] G. Kells, D. Meidan, and P. W. Brouwer, *Phys. Rev. B* **86**, 100503 (2012).
  - [31] E. J. H. Lee, X. Jiang, M. Houzet, R. Aguado, C. M. Lieber, and S. De Franceschi, arXiv:1302.2611 (2013).
  - [32] D. I. Pikulin, J. P. Dahlhaus, M. Wimmer, H. Schomerus, and C. W. J. Beenakker, *New J. Phys.* **14**, 125011 (2012).
  - [33] M. Leijnse, *New J. Phys.* **16**, 015029 (2014).
  - [34] R. López, M. Lee, L. Serra, and J. S. Lim, *Phys. Rev. B* **89**, 205418 (2014).
  - [35] A. Dhar, *Adv. Phys.* **57**, 457 (2008).
  - [36] Y. Dubi and M. Di Ventra, *Rev. Mod. Phys.* **83**, 131 (2011).
  - [37] L. W. Molenkamp, Th. Gravier, H. van Houten, O. J. A. Buijk, M. A. A. Mabesoone, and C. T. Foxon, *Phys. Rev. Lett.* **68**, 3765 (1992).
  - [38] A. S. Dzurak, C. G. Smith, C. H. W. Barnes, M. Pepper, L. Martín-Moreno, C. T. Liang, D. A. Ritchie, and G. A. C. Jones, *Phys. Rev. B* **55**, 10197(R) (1997).
  - [39] S. F. Godijn, S. Möller, H. Buhmann, L. W. Molenkamp, and S. A. van Langen, *Phys. Rev. Lett.* **82**, 2927 (1999).
  - [40] P. N. Butcher, *J. Phys. Condens. Matter* **2**, 4869 (1990).
  - [41] P. Coleman, J. B. Marston, and A. J. Schofield, *Phys. Rev. B* **72**, 245111 (2005).
  - [42] Ph. Jacquod, and R. Whitney, *Europhys. Lett.* **91**, 67009 (2010).
  - [43] V. Balachandran, R. Bosisio, and G. Benenti, *Phys. Rev. B* **86**, 035433 (2012).
  - [44] B. Kubala, J. König, and J. Pekola, *Phys. Rev. Lett.* **100**, 066801 (2008).
  - [45] M. Lee, J. S. Lim, and R. López, *Phys. Rev. B* **87**, 241402 (2013).
  - [46] M. Leijnse and K. Flensberg, *Phys. Rev. Lett.* **107**, 210502 (2011).

- [47] L. Fu and C. L. Kane, Phys. Rev. Lett. **100**, 096407 (2008).
- [48] J. D. Sau, R. M. Lutchyn, S. Tewari, and S. Das Sarma, Phys. Rev. B **104**, 040502 (2010).
- [49] A. Y. Kitaev, Physics-Uspekhi **44**, 131 (2001).
- [50] K. Flensberg, Phys. Rev. B **82**, 180516 (2010).
- [51] D. Sticlet, C. Bena, and P. Simon, Phys. Rev. Letts. **108**, 096802 (2012).
- [52] K. G. Wilson, Rev. Mod. Phys. **47**, 773 (1975).
- [53] H. R. Krishna-murthy, J. W. Wilkins, and K. G. Wilson, Phys. Rev. B **21**, 1003 (1980); **21**, 1044 (1980)
- [54] R. Bulla, T. A. Costi, and T. Pruschke, Rev. Mod. Phys. **80**, 395 (2008).
- [55] W. Hofstetter, Phys. Rev. Lett. **85**, 1508 (2000)
- [56] V. L. Campo and L. N. Oliveira, Phys. Rev. B **72**, 104432 (2005).
- [57] R. Žitko and T. Pruschke, Phys. Rev. B **79**, 085106 (2009).
- [58] R. Bulla, T. A. Costi, and D. Volhardt, Phys. Rev. B **64**, 045103 (2001).
- [59] D. E. Liu and H. U. Baranger, Phys. Rev. B **84**, 201308 (2011).
- [60] T. A. Costi and V. Zlatić, Phys. Rev. B **81**, 235127 (2010).
- [61] R. Schelbner, H. Buhmann, D. Reuter, M. N. Kliselev, and L. W. Molenkamp, Phys. Rev. Lett **95**, 176602 (2005).
- [62] A. C. Hewson, *The Kondo Problem to Heavy-Fermions* (Cambridge University Press, Cambridge, 1993).